ACS OMEGA

http://pubs.acs.org/journal/acsodf

Article

Effects of Fine MgO-Bearing Flux on the Strength of Sinter before and after Low-Temperature Reduction

Haiwei An, Fengman Shen,* Xin Jiang, Yulu Zhou, Haiyan Zheng, and Qiangjian Gao

Cite This: *ACS Omega* 2022, 7, 8686−8696

Read Online

ACCESS | Metrics & More | Article Recommendations

ABSTRACT: Decreasing the MgO content can improve most of the metallurgical properties of sinter, but the low-temperature reduction disintegration index (RDI) property will be worse. In order to improve the RDI property of sinter under certain MgO contents, the effects of fine MgO-bearing flux on the strength of sintered samples before and after reduction in three systems (Fe_2O_3-MgO, Fe_2O_3-MgO-CaO, and Fe_2O_3-MgO-CaO-SiO_2) were investigated in the present work. The experimental results show that (1) in the three systems, the percentage of fine light calcined magnesite (LCM) increases from 0 to 100%, and the compression strength of the samples before reduction increases from 0.140 to 0.187 MPa, from 0.115 to 0.175 MPa, and from 0.121 to 0.164 MPa, respectively. The compression strength of the samples after reduction increases from 0.062 to 0.151 MPa, from 0.100 to 0.156 MPa, and from 0.099 to 0.151 MPa, respectively. (2) The fundamental reason is that the fine powders can increase the specific surface area and the surface energy of the interface. It is beneficial to promoting the mineralization of MgO-bearing flux. More formation of $MgO{\cdot}Fe_2O_3$ may increase the strength of samples before reduction. Less transformation from Fe_2O_3 to Fe_3O_4 may increase the strength of samples after reduction. The microstructures of samples are more compact and uniform. Therefore, fine LCM can improve the strength of sinter before and after reduction. The outcomes of the present work can improve the sintering quality by using the fine MgO-bearing flux in the sintering process.

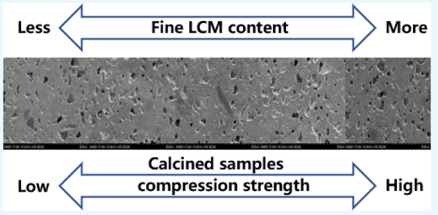

1. INTRODUCTION

Slag-making is an essential link in blast furnace (BF) ironmaking. The properties of BF slag have a significant influence on the output of the hot metal. MgO is one of the essential components of BF slag. A proper MgO content can ensure the fluidity and desulfurization ability of BF slag, especially for slag with a high content of Al_2O_3.[1−7] Usually, the method of adding MgO into BF slag is to add MgO-bearing flux into sintering raw materials. Sinter is the main raw material for BF operation, especially in China, and usually, the proportion of sinter in the burden composition is above 75%,[8−10] and its cold strength and the low-temperature reduction disintegration index (RDI) are important indices for its quality.[11,12] The quality of the sinter not only affects the gas permeability of the upper part of the BF and the smooth operation of the BF[13−18] but also has a significant impact on the energy consumption. Therefore, the influence of MgO on the metallurgical properties of sinter has been widely reported.[7,19,20]

Yang *et al.*[21] reported that the addition of MgO restrained the formation of $CaO{\cdot}Fe_2O_3$ leading to the decrease in the amount of the SFCA (silico-ferrite of calcium and aluminum) bonding phase during the sintering process. Pan *et al.*[22] reported that a low MgO content can effectively improve the reduction rate of sinter. Low-MgO addition not only improves the softening-melting characteristics of the sinter[12,23−25] but also reduces the fuel rate, sintering rate, reducibility, and sinter strength as well as increase the initial melt-down temperature.[26−29] Based on the above studies, no or little addition of MgO in the sinter can effectively improve the efficiency of sintering production and get sinter with high cold strength.[27,28] However, MgO has a positive effect on the RDI property of sinter.[30−33] Therefore, how do we produce the low-MgO sinter with a good RDI property?[34] It is a challenge in the sintering field recently. There are two key points for this challenge: (1) MgO-bearing flux fully plays the positive role for the DRI and (2) tries to avoid the negative effect of MgO on the strength of sinter. However, to the best knowledge of the authors, there are few reports on these two challenges and few methods by which one can obtain low-MgO sinter with a good RDI property.

Based on our previous work, ground MgO-bearing flux may increase the specific surface area of the interface and the surface energy. This is beneficial to the effective mineralization of MgO-bearing flux, which is important to the strength and the RDI property of sinter. Therefore, in the present

Received: November 29, 2021
Accepted: February 1, 2022
Published: March 1, 2022

https://doi.org/10.1021/acsomega.1c06722
ACS Omega 2022, 7, 8686−8696

work, the effects of fine MgO-bearing flux on the strength before and after low-temperature reduction were investigated. The main research contents and originalities included the following:

(1) Compared with the traditional method, MgO-bearing flux was first ground and then added into raw sintering materials.
(2) The effects of the amount of fine MgO-bearing flux on the strength of samples before and after low-temperature reduction were investigated.
(3) The micrographs of samples in three systems (Fe_2O_3-MgO, Fe_2O_3-MgO-CaO, and Fe_2O_3-MgO-CaO-SiO_2) with different amounts of fine MgO-bearing flux were analyzed and discussed. The outcomes of the present work can improve the sintering quality by using the fine MgO-bearing flux in the sintering process.

2. EXPERIMENTAL METHODS

Raw materials included pure chemical reagents Fe_2O_3, CaO, and SiO_2 and industrial flux (light calcined magnesite, shortened to LCM). The chemical compositions of the LCM were obtained by chemical analyses, which are listed in Table 1. The main component of LCM was MgO (MgO = 71.35%). The particle size of magnesite was the only variable in the experiment: coarse LCM was supplied by a steel enterprise in China, and fine LCM was obtained by grinding of coarse LCM. Figure 1 shows the size distribution of these two kinds of LCM. The median size of coarse LCM was 143 μm, and the median size of fine LCM was 46.8 μm.

Table 1. Chemical Composition of Light Calcined Magnesite (LCM) (Mass %)

MgO	CaO	SiO_2	Al_2O_3	LOI
71.35	2.76	5.78	0.74	17.84

The experimental procedure was as follows:

(1) For sample preparation, the samples were designed as the Fe_2O_3-MgO system, the Fe_2O_3-MgO-CaO system, and the Fe_2O_3-MgO-CaO-SiO_2 system listed in Table 2. The reasons for choosing these compositions were as follows.
   (a) In the present work, the main focus is MgO, and MgO mainly reacts with Fe_2O_3 to form MgO·Fe_2O_3. Therefore, the Fe_2O_3-MgO system was designed.
   (b) In order to compare the formation between MgO·Fe_2O_3 and CaO·Fe_2O_3, the Fe_2O_3-MgO-CaO system was designed.
   (c) The main composition of the bonding phase in real sintered ores includes Fe_2O_3, CaO, MgO, and SiO_2, so the Fe_2O_3-MgO-CaO-SiO_2 system was designed too.

   The weighted chemical reagents according to Table 2 were fully mixed in an agate mortar. Then, they were pressed into briquettes (8 mm in diameter and 5 mm in height) by using a briquetting machine at a pressure of 12 MPa for 3 min. The weight of each sample was about 1 g.
(2) For sample calcination, the previous samples were calcined at 1250 °C for 20 min. The sample obtained by calcination was named as the "sample before reduction" in the present work.

   For the calcination temperature, the sample cannot produce too much liquid phase during calcination. Otherwise, the strength cannot be measured. Therefore, the calcination temperature was lower than the actual sintering temperature, and 1250 °C was selected.

   For the calcination time, two reasons were considered: (a) The time was short, the mineralization reaction was slow, and the experimental results were not obvious. In order to make the experimental results obvious, we chose a longer time, 20 min. (b) The calcination temperature (1250 °C) of the experiment was lower than the actual sintering temperature (1300−1400 °C). Therefore, the calcination time was prolonged to 20 min for promoting the mineralization effect.
(3) For sample reduction, part of the calcined sample was reduced by a reducing gas in a Tammann furnace. The experimental conditions in this paper refer to GB/T 3242-91. Figure 2 shows the schematic diagram of test equipment. The main body of equipment was mainly composed of a heating shaft furnace and a reaction tube. The reaction tube height was 800 mm, and the

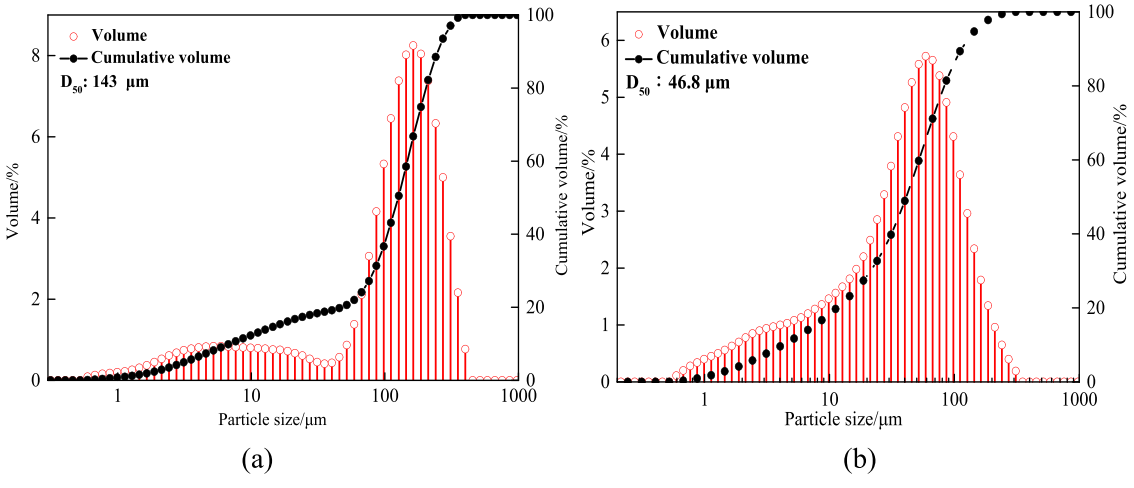

Figure 1. LCM particle size distribution: (a) coarse LCM and (b) fine LCM.

https://doi.org/10.1021/acsomega.1c06722
ACS Omega 2022, 7, 8686−8696

Table 2. Experimental Scheme of Sample Preparation

group	no.	Fe_2O_3 (mol) /weight (g)	MgO (mol) /weight (g)	CaO (mol) /weight (g)	SiO_2 (mol) /weight (g)	coarse magnesite (%) /weight (g)	fine magnesite (%) /weight (g)
1	1-1	1/0.799	1/0.201			100/0.201	0/0
	1-2	1/0.799	1/0.201			75/0.151	25/0.050
	1-3	1/0.799	1/0.201			50/0.100	50/0.101
	1-4	1/0.799	1/0.201			25/0.050	75/0.151
	1-5	1/0.799	1/0.201			0/0	100/0.201
2	2-1	1/0.624	1/0.157	1/0.219		100/0.157	0/0
	2-2	1/0.624	1/0.157	1/0.219		75/0.118	25/0.039
	2-3	1/0.624	1/0.157	1/0.219		50/0.078	50/0.079
	2-4	1/0.624	1/0.157	1/0.219		25/0.039	75/0.118
	2-5	1/0.624	1/0.157	1/0.219		0/0	100/0.157
3	3-1	2/0.558	2/0.141	2/0.196	1/0.105	100/0.141	0/0
	3-2	2/0.558	2/0.141	2/0.196	1/0.105	75/0.106	25/0.035
	3-3	2/0.558	2/0.141	2/0.196	1/0.105	50/0.070	50/0.071
	3-4	2/0.558	2/0.141	2/0.196	1/0.105	25/0.035	75/0.106
	3-5	2/0.558	2/0.141	2/0.196	1/0.105	0/0	100/0.141

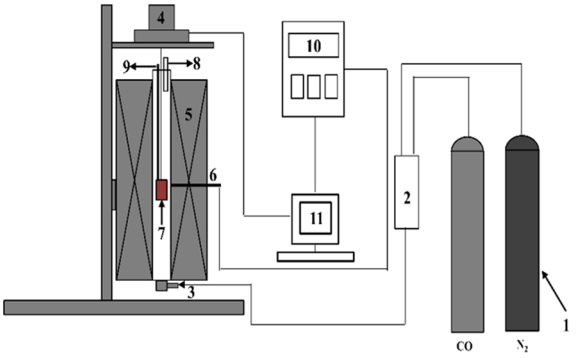

Figure 2. Schematic diagram of the reduction disintegration experiment.

inner diameter of the reaction tube was 75 mm. The reduction temperature, atmosphere, and time are shown in Table 3. The reduced sample was named as the "sample after reduction".

Table 3. Reduction Experimental Conditions

temperature	gas composition	gas flow	time
500 °C	20% CO+20% CO_2+60% N_2	15 L/min	1 h

(4) For compression strength tests, the compression strengths of the sample before reduction and the sample after reduction were tested. The compression strength of the sample after reduction was used as an index to evaluate the RDI in present work.

(5) For XRD tests, a part of the sample before reduction and the sample after reduction was ground into a fine powder using an agate mortar and pestle and then sieved completely through a 325 mesh sieve. Then, powder XRD analyses were carried out using an X-ray diffractometer. Cu Kα was used as the radiation source (40 kV, 400 mA) with a graphite monochromator in the diffraction beam path. The XRD data were collected by using the continuous scanning mode, of which the scanning speed was maintained at 10°/min.

(6) For morphology tests, the remaining part of the samples was polished by setting them into ethylenediamine-doped epoxy resin for the preparation for SEM-EDS analyses. SEM was performed using a scanning electron microscope. The accelerating voltage was 20 kV. Energy-dispersive spectroscopy (EDS) was performed on the same instrument.

(7) For sintering pot tests, in order to confirm the results of the above model samples, the sintering pot experiments were carried out in sintering equipment of the Iron-making Institute of Northeast University in China. The sintering raw materials used in this test were from a Chinese iron and steel enterprise, including blended ore, return ore, dolomite, quicklime, coke, outsourced coke, fly ash, etc. The ore-matching scheme of the sintering pot test is shown in Table 4. In the test, dolomite was used as MgO-bearing flux, the proportion was fixed, and the variable was the proportions of finely ground dolomite powder of 1 mm, which are 0 (i.e., the not ground dolomite powder particle size was 3 mm), 50, and 100%. In addition, for a quantitative consideration of the strength degradation because of reduction, the reduction rate of sinter was tested under RDI test conditions.

Table 4. Ore-Matching Scheme of the Sintering Pot Test (Mass %)

	blended ore	return mine	dolomite	quicklime	coke	outsourced coke	fly ash	fine dolomite
no. 1	66.63	15.57	3.53	8.69	2.70	1.23	1.64	0
no. 2	66.63	15.57	3.53	8.69	2.70	1.23	1.64	50
no. 3	66.63	15.57	3.53	8.69	2.70	1.23	1.64	100

https://doi.org/10.1021/acsomega.1c06722
ACS Omega 2022, 7, 8686−8696

3. EXPERIMENTAL RESULTS

3.1. Experimental Results of Model Samples. Figure 3 shows the compression strength of the sample before

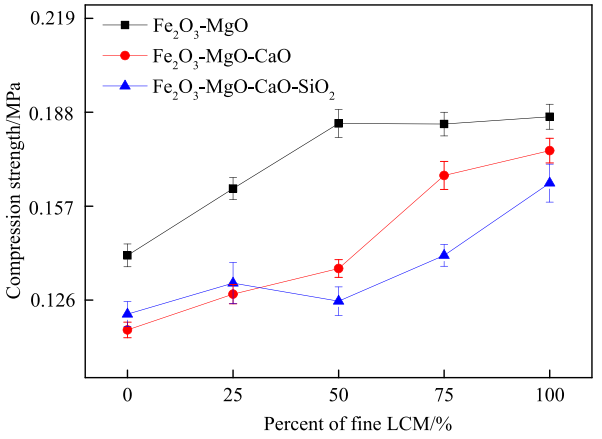

Figure 3. Compression strength of samples before reduction.

reduction. As the percentage of fine LCM increases from 0 to 100%, the compression strength of the sample in the Fe_2O_3-MgO system increases from 0.142 to 0.186 MPa, the compression strength of the sample in the Fe_2O_3-MgO-CaO system increases from 0.115 to 0.175 MPa, and the compression strength of the sample in the Fe_2O_3-MgO-CaO-SiO_2 system increases from 0.121 to 0.164 MPa. Among the three systems, the strength of the Fe_2O_3-MgO system is obviously higher than those of the other two systems. The reason is that there is some liquid phase formed in Fe_2O_3-MgO-CaO and Fe_2O_3-MgO-CaO-SiO_2 systems (refer to Figures 8 and 10 in Section 4). The liquid phase becomes a glass phase during the rapid cooling, which can result in low strength for these two systems.

Figure 4 shows the compression strength of samples after reduction. In the three systems, the percentage of fine LCM

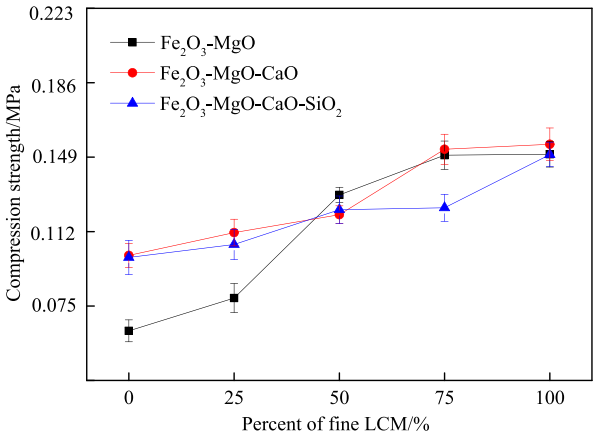

Figure 4. Compression strength of samples after reduction.

increases from 0 to 100%, and the compression strength of the sample after reduction increases from 0.062 to 0.150 MPa, from 0.100 to 0.156 MPa, and from 0.099 to 0.151 MPa, respectively. Among the three systems, in the case of low fine LCM addition (0 and 25%), the strength of the Fe_2O_3-MgO system is the lowest. The reason is that less MgO·Fe_2O_3 formed during calcination, and then, more Fe_2O_3 is reduced to Fe_3O_4 during reduction, which can result in a lower strength after reduction. In the case of high fine LCM addition (75 and 100%), more MgO·Fe_2O_3 formed during calcination in the three systems. Then, the strength of the three systems is similar.

3.2. XRD and SEM Analyses on the Sample before Reduction. *3.2.1. Fe_2O_3-MgO System Sample before Reduction.* Figure 5 shows XRD patterns of the Fe_2O_3-

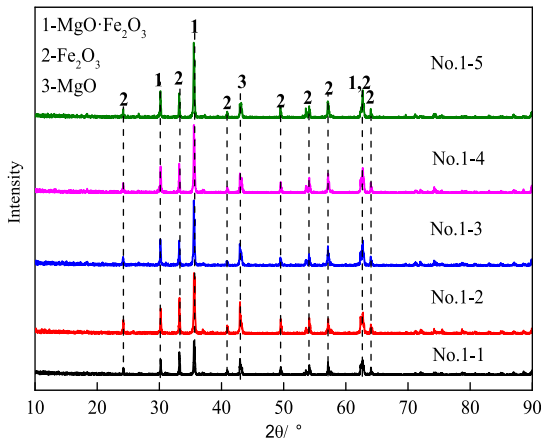

Figure 5. XRD patterns of the Fe_2O_3-MgO system sample before reduction.

MgO sample before reduction. The major mineral components in the sample are Fe_2O_3, MgO, and MgO·Fe_2O_3. With the increase of fine LCM, the peak value of MgO·Fe_2O_3 becomes higher and the peak value of MgO decreases, which shows that the content of MgO·Fe_2O_3 increases and the content of MgO decreases. The reason is that some MgO reacts with Fe_2O_3 to form MgO·Fe_2O_3 in the sample before reduction, but some unreacted MgO still exists in the sample. Especially when adding a small amount of the fine LCM in the sample, the unreacted MgO is higher. Therefore, the increase of fine LCM promotes the mineralization reaction in the system, and the decrease in the content of unreacted MgO is beneficial to the strength of the sample before reduction.

Figure 6 shows the SEM images and EDS analyses of the Fe_2O_3-MgO system sample before reduction. The focus in the present work is the mineralization of MgO. Therefore, the mineralization reaction between MgO and Fe_2O_3, the products of the reaction, and unreacted MgO were mainly analyzed. Basically, there are two phases in this sample, (a) the unreacted MgO phase represented by point 1 and point 3 and (b) MgO·Fe_2O_3 represented by point 2. It can be seen that with the increase of fine LCM, the microstructure of the sample has an obvious difference. With the increase of fine LCM, the size of unreacted MgO particles is smaller because more MgO reacts with Fe_2O_3 to form MgO·Fe_2O_3. Therefore, the mineralization reaction between MgO and Fe_2O_3 is enhanced during the calcination process due to the increase in the specific surface area and surface energy of fine LCM (details can be found in Section 4 "Discussion"). Then, the structure of the sample becomes more uniform and compact, and this is the key to the increase in the compression strength of the sample before reduction with the increase of fine LCM in the Fe_2O_3-MgO system.

https://doi.org/10.1021/acsomega.1c06722
ACS Omega 2022, 7, 8686−8696

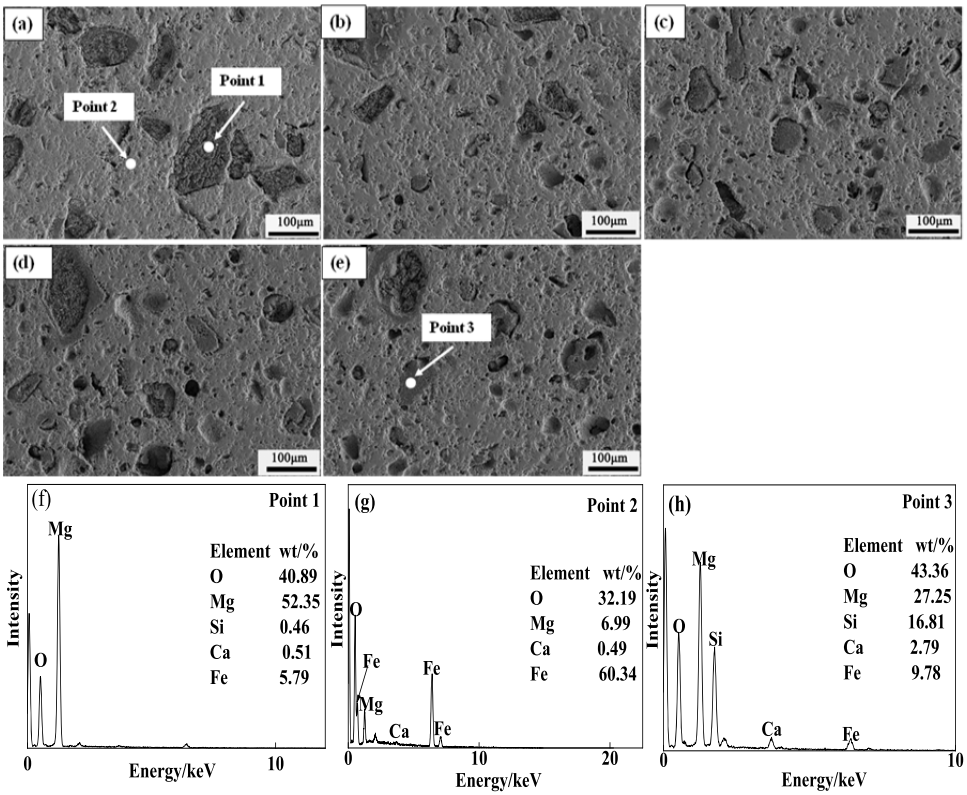

Figure 6. SEM images of (a) 0, (b) 25, (c) 50, (d) 75, and (e) 100% fine LCM and EDS analyses of (f) point 1, (g) point 2, and (h) point 3 in the Fe_2O_3-MgO system sample before reduction.

3.2.2. Fe_2O_3-MgO-CaO System Sample before Reduction. Figure 7 shows XRD patterns of the Fe_2O_3-MgO-CaO system

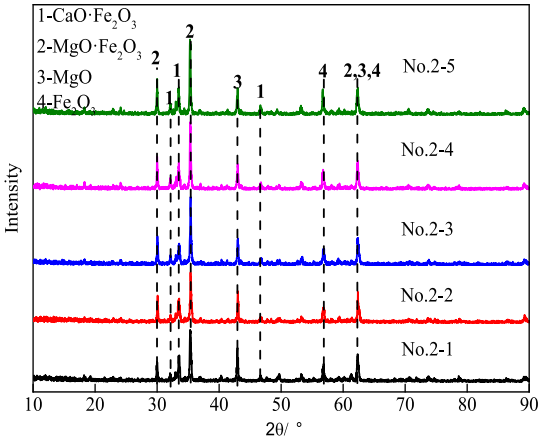

Figure 7. XRD patterns of the Fe_2O_3-MgO-CaO system sample before reduction.

sample before reduction. The major mineral components in the sample are $MgO{\cdot}Fe_2O_3$, $CaO{\cdot}Fe_2O_3$, Fe_2O_3, and MgO. With the increase of fine LCM, the content of $MgO{\cdot}Fe_2O_3$ increases and the content of unreacted MgO decreases.

Figure 8 shows the SEM images and EDS analyses of the Fe_2O_3-MgO-CaO system sample before reduction. Similar to Figure 6, the mineralization reaction between MgO and other oxides, the products of the reaction, and unreacted MgO were mainly analyzed. Compared with the Fe_2O_3-MgO system, there is some $CaO{\cdot}Fe_2O_3$ liquid phase (point 5) in the Fe_2O_3-MgO-CaO system sample because the melting point of $CaO{\cdot}Fe_2O_3$ is low (the lowest melting point at the eutectic point is only about 1200 °C). Also, the unreacted MgO phase (point 4) decreases (consistent with the XRD analyses). Similarly, with the increase of fine LCM, the size of unreacted MgO particles is smaller because more MgO reacts with Fe_2O_3 to form $MgO{\cdot}Fe_2O_3$ and more MgO dissolves into the $CaO{\cdot}Fe_2O_3$ liquid phase. The mineralization among MgO, Fe_2O_3, and CaO is further enhanced in the calcination process. Then, the structure of the sample becomes more uniform and compact, and this is the key to the increase in the compression strength of the sample before reduction with the increase of fine LCM in the Fe_2O_3-MgO-CaO system.

3.2.3. Fe_2O_3-MgO-CaO-SiO_2 Sample before Reduction. Figure 9 shows XRD patterns of the Fe_2O_3-MgO-CaO-SiO_2 system sample before reduction. The major mineral components in the sample are $MgO{\cdot}Fe_2O_3$, $CaO{\cdot}Fe_2O_3$, $2CaO{\cdot}Fe_2O_3$, Fe_2O_3, and MgO. With the increase of fine LCM, the peak intensity of $MgO{\cdot}Fe_2O_3$ becomes higher and the content increases. Therefore, the unreacted MgO is relatively less. There is no obvious change in other phases from the XRD diagram. Since the melting point of SiO_2 is low, there is a plurality of liquid phases. These factors are beneficial to the improvement of the strength.

Figure 10 shows SEM images and EDS analyses of the sample in the Fe_2O_3-MgO-CaO-SiO_2 system before reduction. Similar to Figures 6 and 8, with the increase of fine LCM, the mineralization effect between substances enhances obviously and the pores on the surface of the sample become compact.

3.3. XRD and SEM Analyses on the Samples after Reduction. *3.3.1. Fe_2O_3-MgO System Sample after Reduction.* Figure 11 shows XRD diagrams of the Fe_2O_3-

https://doi.org/10.1021/acsomega.1c06722
ACS Omega 2022, 7, 8686−8696

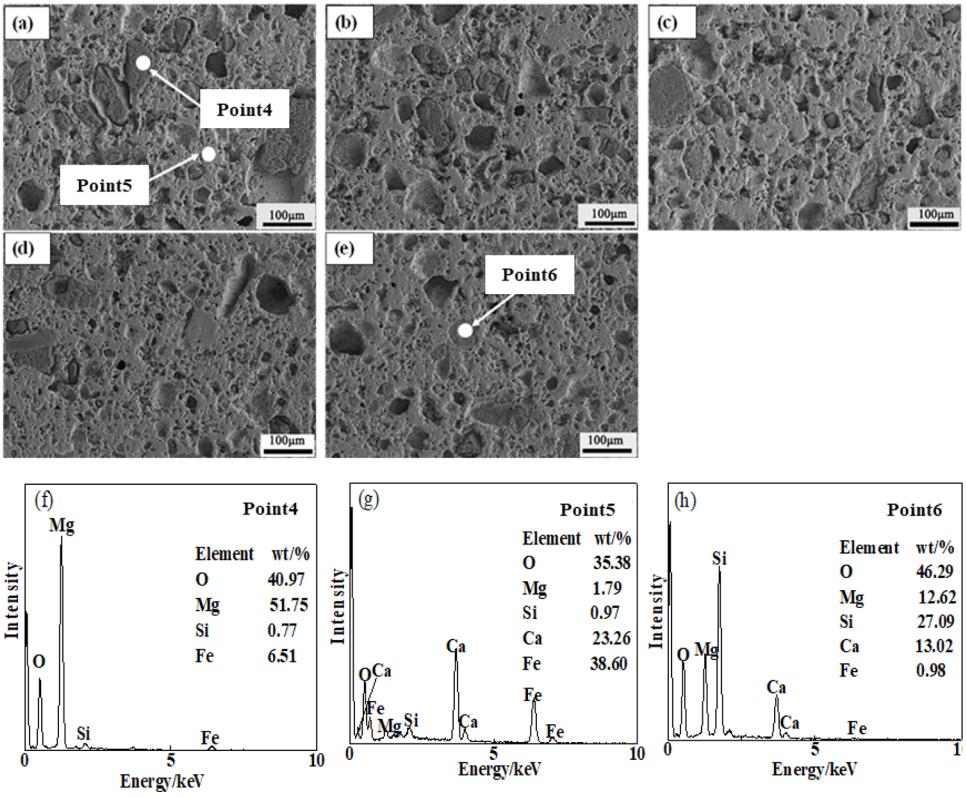

Figure 8. SEM images of (a) 0, (b) 25, (c) 50, (d) 75, and (e) 100% fine LCM and EDS analyses of (f) point 4, (g) point 5, and (h) point 6 in the Fe_2O_3-MgO-CaO system sample before reduction.

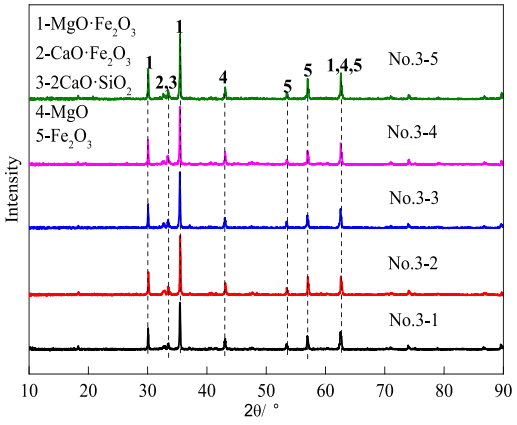

Figure 9. XRD patterns of the Fe_2O_3-MgO-CaO-SiO_2 system sample before reduction.

MgO system sample after reduction. The major phases are Fe_3O_4, MgO·Fe_2O_3, Fe_2O_3, and MgO. With the increase of fine LCM, the peak intensity of MgO·Fe_2O_3 becomes higher and the peak intensity of MgO becomes lower. The reason is that fine LCM can promote mineralization, resulting in the Fe_2O_3 content decrease. The decrease in the Fe_2O_3 content inhibits the transformation of Fe_2O_3 to Fe_3O_4 and the volume expansion. Therefore, fine LCM is beneficial to improving the sample strength.

Figure 12 shows SEM analyses of the Fe_2O_3-MgO system sample after reduction. EDS analyses are shown in Table 5. In the case of no fine LCM, the mineralization reaction is relatively poor, and the sample contains more MgO (point 10) and Fe_2O_3 (point 11). Under the reducing atmosphere, more Fe_3O_4 is generated, resulting in the lower compression strength of the sample. When adding 25% of fine LCM, the matrix still contains more Fe_3O_4 (point 12) and the compression strength changes little. With the increase of fine LCM, the mineralization effect enhances obviously and more MgO·Fe_2O_3 (point 14) forms in the sample. Therefore, the high content of fine LCM is beneficial to the compression strength.

3.3.2. Fe_2O_3-MgO-CaO System Sample after Reduction. Figure 13 shows XRD analyses of the sample in the Fe_2O_3-MgO-CaO system after reduction. The major phases are Fe_2O_3, Fe_3O_4, MgO, 2CaO·Fe_2O_3, and MgO·Fe_2O_3. With the increase of the fine LCM, the peak intensity of MgO·Fe_2O_3 becomes higher. The content of MgO·Fe_2O_3 increases and the Fe_3O_4 content decreases in the sample. The reason is that fine LCM increases the specific surface area of the interface, enhances surface energy, and enhances mineralization. Therefore, fine LCM inhibits the Fe_2O_3 reduction to Fe_3O_4. This is beneficial to improving the strength of the sample.

Figure 14 shows SEM analyses of the sample in the Fe_2O_3-MgO-CaO system after reduction. EDS analyses are shown in Table 6. Without the addition of fine LCM, a small amount of MgO (point 17) distributed between MgO·Fe_2O_3 and Fe_3O_4 (point 16). With the increase of fine LCM, the unreacted MgO decreases and the crystallinity of the sample improves. 2CaO·Fe_2O_3 (point 19) distributed between MgO·Fe_2O_3 and Fe_3O_4. Therefore, with the increase of fine LCM, the mineralization enhances. Inhibiting the transition from Fe_2O_3 to Fe_3O_4 is beneficial to improving the compression strength of the sample.

https://doi.org/10.1021/acsomega.1c06722
ACS Omega 2022, 7, 8686−8696

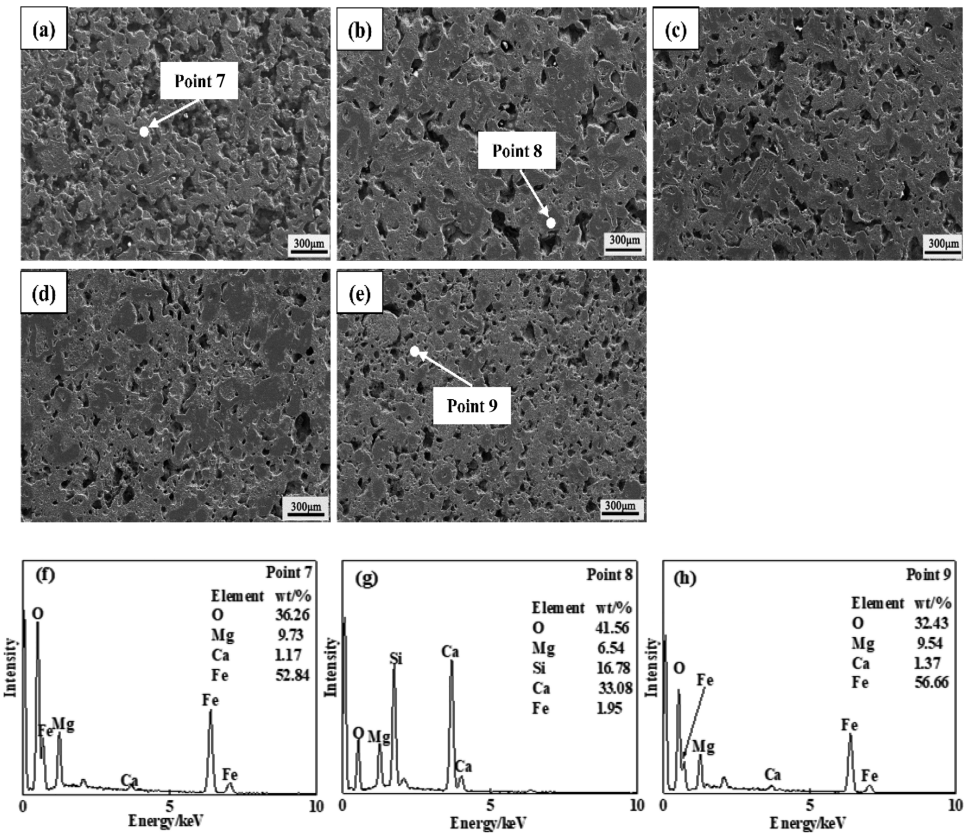

Figure 10. SEM images of (a) 0, (b) 25, (c) 50, (d) 75, and (e) 100% fine LCM and EDS analyses of (f) point 7, (g) point 8, and (h) point 9 in the Fe_2O_3-MgO-CaO-SiO_2 system sample before reduction.

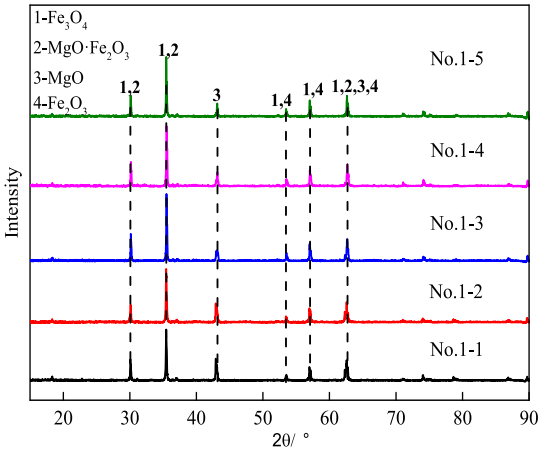

Figure 11. XRD patterns of the Fe_2O_3-MgO system sample after reduction.

3.3.3. Fe_2O_3-MgO-CaO-SiO_2 System Sample after Reduction. Figure 15 shows the XRD analyses of the sample in the Fe_2O_3-MgO-CaO-SiO_2 system after reduction. The major phases are Fe_3O_4, Fe_2O_3, MgO, $MgO{\cdot}Fe_2O_3$, $2FeO{\cdot}SiO_2$, MgO, and $2CaO{\cdot}Fe_2O_3$. Compared with the other series of the sample, $2FeO{\cdot}SiO_2$ appeared in the Fe_2O_3-MgO-CaO-SiO_2 system, and with the increase of fine LCM, the $2FeO{\cdot}SiO_2$ increased and the change of other phases were consistent with the other series of the sample. Therefore, the same conclusion can be drawn: fine LCM can effectively enhance the mineralization, increase the strength, and improve the RDI of the sinter.

Based on the previous analyses, the microstructure changes of the samples were similar, so the samples of the Fe_2O_3-MgO-CaO-SiO_2 system were not analyzed by SEM-EDS.

3.4. Experimental Results of the Sintering Pot. The sintering pot test results are shown in Table 7. With the fine dolomite increases from 0 to 100%, the tumbler index of sinter increases slightly from 74.93 to 75.33%. The RDI of sinter increases from 83.75 to 87.41%. However, the increase in the RDI slows down when the fine dolomite exceeds 50%. With the increase of fine dolomite from 0 to 100%, the RI (reducibility index) of sinter after reduction is 8.7, 5.2, and 4.6%. The decrease in the RI obviously slows down when the fine dolomite exceeds 50%. The high RDI corresponds to a low RI, which shows the strength degradation of sinter because of reduction. This confirmed the results of the model samples. Therefore, the fine dolomite is beneficial to forming $MgO{\cdot}Fe_2O_3$ and decreases the reduction rate of sinter and then improves the RDI property of sinter.

4. DISCUSSION

In order to clarify the fundamentals of the effects of fine LCM on the strength of samples before and after reduction, elaborate discussion was carried out, including the specific surface area and surface energy analysis and the mineral components in the model samples before and after reduction.

4.1. Specific Surface Area and Surface Energy Analysis. The size of coarse/fine LCM is different, and the specific surface area and the surface energy are different too. Supposing that the LCM particles are spherical, then, the specific surface area can be obtained according to eq 1. The surface energy can be obtained according to eq 2.

https://doi.org/10.1021/acsomega.1c06722
ACS Omega 2022, 7, 8686−8696

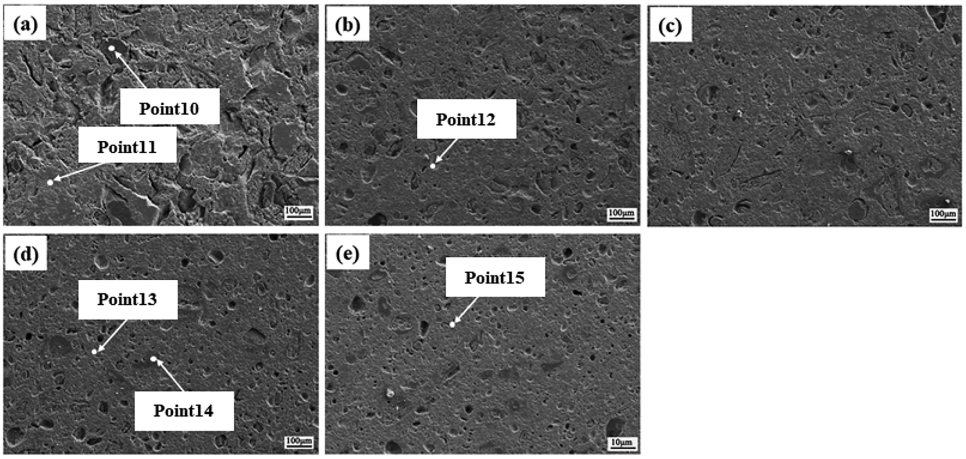

Figure 12. SEM images of (a) 0, (b) 25, (c) 50, (d) 75, and (e) 100% fine LCM in the Fe_2O_3-MgO system sample after reduction.

Table 5. EDS Analyses of the Fe_2O_3-MgO System Sample after Reduction (Mass %)

zone	Mg	Fe	O	Si	Ca
point 10	57.23	1.99	40.77		
point 11	1.18	68.94	29.87		
point 12	7.01	62.35	30.64		
point 13	9.27	58.07	32.66		
point 14	27.62	10.17	44.43	15.45	2.33
point 15	8.79	58.86	32.35		

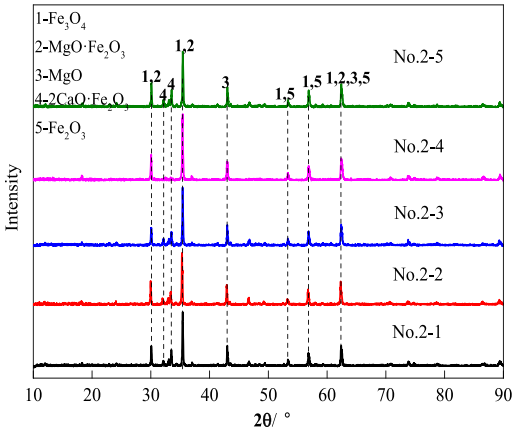

Figure 13. XRD patterns of the Fe_2O_3-MgO-CaO system sample after reduction.

$$S = \frac{s}{M} \tag{1}$$

where S is the specific surface area, s is the surface area, and M is the mass.

$$E^{\gamma} = \frac{1}{2}s \times E \tag{2}$$

where E^{γ} is the surface energy, s is the surface area, and E is the sum of all bond energies per unit surface area (the bond energy of the same material is a constant; here, $E = 1$ is assumed).

Then, the specific surface area and surface energy of coarse/fine LCM were obtained and are listed in Table 8. From the table, it can be seen that fine LCM has a larger specific surface area and surface energy than the coarse LCM. In the present work (Figure 1), the diameter of LCM particles decreases from 143 (median size of coarse LCM) to 46.8 μm (median size of fine LCM), the specific surface area of LCM increases from 15.541 to 47.44 $m^2 \cdot g^{-1}$, and the surface energy per unit mass increases from 7.771 to 23.724 J. The increase in surface energy is the fundamental and key point for the mineralization and increasing the strength of samples.

4.2. Mineral Components of Samples before Reduction. The effects of increasing the percentages of fine LCM on the mineral components of the samples confirmed by X-ray diffraction and EDS results are shown in Table 9.

In the present work, the primary focus is MgO, and the main reaction during calcination (before reduction) is the mineralization reaction between MgO and Fe_2O_3 to form $MgO \cdot Fe_2O_3$. Therefore, the change in the $MgO \cdot Fe_2O_3$ content is the key point for the strength of samples before reduction. It can be seen from Table 9 that with the increase of fine LCM, the content of $MgO \cdot Fe_2O_3$ in the samples before reduction in the three systems increases and the free MgO decreases. For example, in the case of fine LCM = 100%, MgO was not found in the three systems by the EDS test. The reason is that more fine LCM increases the specific surface area and the surface energy, which can enhance the mineralization between MgO and Fe_2O_3, and then, most of MgO has reacted with Fe_2O_3 to form more $MgO \cdot Fe_2O_3$, and the unreacted MgO is very little. Consequently, it results in a compact structure.

Therefore, the main reason for that the strength of the sample with high fine LCM increases before reduction is that the mineralization reaction between MgO and Fe_2O_3 is enhanced by the higher specific surface area and the surface energy, and hence, more $MgO \cdot Fe_2O_3$ is formed. This is beneficial to the strength of samples before reduction.

4.3. Mineral Components of Samples after Reduction. In the case of low-temperature reduction, the main reaction is the reduction from Fe_2O_3 to Fe_3O_4. Therefore, the change in the Fe_3O_4 content is investigated in the present work, which is the main influencing factor for the strength of the sample after reduction. It can be seen from Table 9 that with the increase of fine LCM, the content of Fe_3O_4 in the samples after reduction in the three systems decreases. For example, at a high percentage of fine LCM, there was no Fe_3O_4 found by the EDS test, and more $MgO \cdot Fe_2O_3$ was

https://doi.org/10.1021/acsomega.1c06722
ACS Omega 2022, 7, 8686−8696

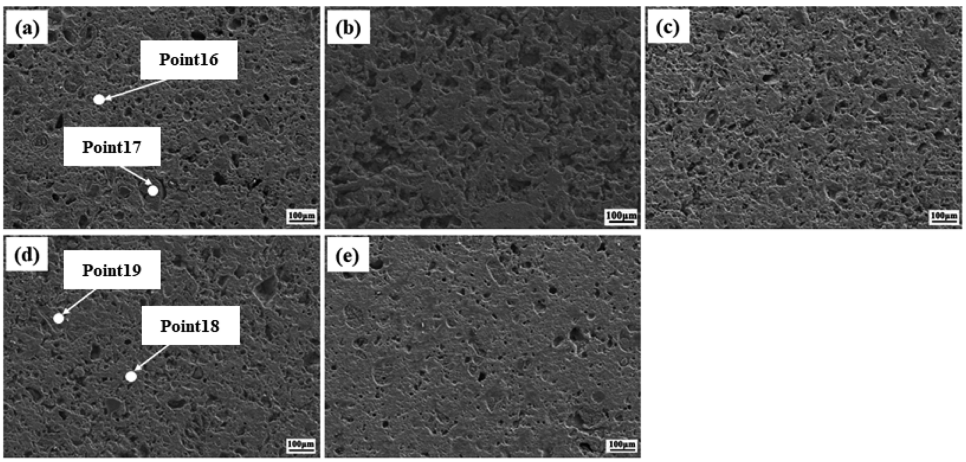

Figure 14. SEM images of (a) 0, (b) 25, (c) 50, (d) 75, and (e) 100% fine LCM in the Fe_2O_3-MgO-CaO system sample after reduction.

Table 6. EDS Analyses of the Fe_2O_3-MgO-CaO System Sample after Reduction (Mass %)

zone	Mg	Fe	O	Si	Ca
point 16	8.19	56.97	33.01		1.84
point 17	60.21	1.01	38.75		
point 18	4.46	40.26	37.62	1.16	16.51
point 19	1.03	35.17	36.10	1.68	26.02

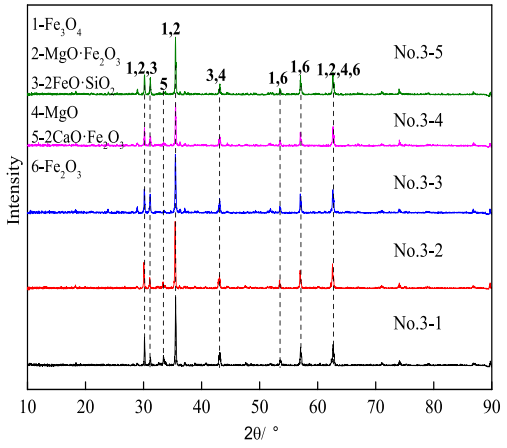

Figure 15. XRD patterns of the Fe_2O_3-MgO-CaO-SiO_2 system sample after reduction.

Table 7. Effect of the Fine Dolomite Proportion on the Sintering Pot Index (Mass %)

fine dolomite	tumbler index	RI	$RDI_{+3.15}$
0	74.93	8.7	83.75
50	76.13	5.2	88.22
100	75.33	4.6	87.41

found. It is well-known that the lattice transformation from Fe_2O_3 to Fe_3O_4 is the main reason for the strength of iron ore decreasing during low-temperature reduction.

Therefore, the main reason for that the strength of the sample with high fine LCM increases after reduction is that more MgO·Fe_2O_3 is present in the samples. MgO·Fe_2O_3 is more stable than Fe_2O_3 and results in a low reduction degree and a low Fe_3O_4 content. Then, the negative effect of lattice transformation from Fe_2O_3 to Fe_3O_4 is partly relieved, and consequently, the strength after reduction is improved.

4.4. Summarization. The fundamentals of the effects of fine LCM on the strength of samples before and after reduction are summarized in Figure 16. Basically, the mechanism may be explained as follows. (1) Fine LCM can increase the specific surface area and surface energy. (2) The mineralization between MgO and Fe_2O_3 is enhanced, and more MgO·Fe_2O_3 is formed. (3) Little unreacted MgO exists in the sample and results in a compact structure; then, the strength before reduction is increased. (4) The reduction degree and the Fe_3O_4 content are decreased because MgO·Fe_2O_3 is more stable than Fe_2O_3, and the lattice transformation is relieved; then, the strength after reduction is increased.

5. CONCLUSIONS

In this work, the effects of fine LCM on the strength of calcination before and after low-temperature reduction were investigated. Based on the laboratory model samples' test, fine LCM can effectively improve the strength of the sample before and after reduction. XRD and SEM-EDS analyses indicate that the strengthening of the mineralization effect is the major reason for the increase in the sample compression strength before and after reduction. Sintering pot test results illustrate that fine dolomite is beneficial to forming MgO·Fe_2O_3 and decreases the reduction rate of sinter and then improves the RDI property of sinter. The results of the sintering pot test also confirm the correctness of model samples. Finally, the theoretical calculation of the specific surface area confirms the correctness of all experimental analyses. The main findings can be summarized as follows.

Table 8. Comparison of Coarse LCM and Fine LCM

LCM	particle diameter (μm)	surface area (m^2)	density (g/m^3)	mass (g)	specific surface area (m^2/g)	surface energy (J/g)
coarse	143	6.42×10^{-8}	2700	4.131×10^{-9}	15.541	7.771
fine	46.8	6.88×10^{-9}	2700	1.450×10^{-10}	47.448	23.724

https://doi.org/10.1021/acsomega.1c06722
ACS Omega 2022, 7, 8686−8696

Table 9. Effect of Increasing the Percentage of Fine LCM on the Sample

	system	items	EDS points	change[a]
samples before reduction	Fe_2O_3-MgO	Fe_2O_3	point 2	↓
		MgO	point 1, point 3	↓
		MgO·Fe_2O_3	point 2	↑
	Fe_2O_3-MgO-CaO	Fe_2O_3		↓
		MgO	point 4	↓
		MgO·Fe_2O_3		↑
		CaO·Fe_2O_3	point 5	↑
	Fe_2O_3-MgO-CaO-SiO_2	Fe_2O_3		↓
		MgO		↓
		MgO·Fe_2O_3	point 7, point 9	↑
		CaO·Fe_2O_3		↑
		2CaO·SiO_2	point 8	↑
samples after reduction	Fe_2O_3-MgO	Fe_2O_3	point 12	↓
		Fe_3O_4	point 11	↓
		MgO	point 10	↓
		MgO·Fe_2O_3	point 13, point 15	↑
	Fe_2O_3-MgO-CaO	Fe_2O_3		↓
		Fe_3O_4		↓
		MgO	point 17	↓
		MgO·Fe_2O_3	point 16	↑
		2CaO·Fe_2O_3	point 18, point 19	↑
	Fe_2O_3-MgO-CaO-SiO_2	Fe_2O_3		↓
		Fe_3O_4		↓
		MgO		↓
		MgO·Fe_2O_3		↑
		2CaO·Fe_2O_3		↑
		2FeO·SiO_2		↑

[a]Notes: ↑ increases; ↓ decreases.

(1) In three systems (Fe_2O_3-MgO, Fe_2O_3-MgO-CaO, and Fe_2O_3-MgO-CaO-SiO_2), the percentage of fine LCM increases from 0 to 100%, and the compression strength of the sample before reduction increases from 0.140 to 0.187 MPa, from 0.115 to 0,175 MPa, and from 0.121 to 0.164 MPa, respectively. The compression strength of the samples after reduction increases from 0.062 to 0.151 MPa, from 0.100 to 0.156 MPa, and from 0.099 to 0.151 MPa, respectively.

(2) The fundamental reason for the effects of fine LCM on the strength of sinter is that the fine powders can increase the specific surface area and the surface energy of the interface. It is beneficial to promoting the mineralization of MgO-bearing flux. Therefore, fine LCM can improve the strength of sinter before and after reduction.

Applying the above findings to the actual sintering production can reduce the use of MgO and produce the low-MgO sinter with a good RDI property. This is of great significance to improve the quality of sinter.

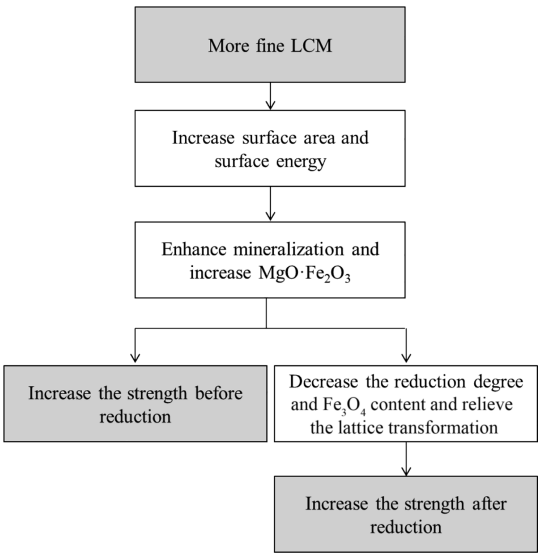

Figure 16. Fundamentals of the effects of fine LCM on the strength of samples before and after reduction.

AUTHOR INFORMATION

Corresponding Author

Fengman Shen − *School of Metallurgy, Northeastern University, Shenyang 110819, P. R. China*; Phone: +8618940219515; Email: shenfm@mail.neu.edu.cn

Authors

Haiwei An − *School of Metallurgy, Northeastern University, Shenyang 110819, P. R. China*; orcid.org/0000-0001-9165-4584

Xin Jiang − *School of Metallurgy, Northeastern University, Shenyang 110819, P. R. China*

Yulu Zhou − *School of Metallurgy, Northeastern University, Shenyang 110819, P. R. China*

Haiyan Zheng − *School of Metallurgy, Northeastern University, Shenyang 110819, P. R. China*

Qiangjian Gao − *School of Metallurgy, Northeastern University, Shenyang 110819, P. R. China*

Complete contact information is available at: https://pubs.acs.org/10.1021/acsomega.1c06722

Notes

The authors declare no competing financial interest.

ACKNOWLEDGMENTS

Financial support from the National Natural Science Foundation of China (NSFC 52074074, NSFC 51874080, NSFC 51974073, NSFC 52074072, and 52074086), the Xingliao Talent Project (XLYC2007152), and the Fundamental Research Funds for the Central Universities (N2125036 and N2125029) is much appreciated.

REFERENCES

(1) Yadav, U. S.; Pandey, B. D.; Das, B. K.; Jena, D. N. Influence of magnesia on sintering characteristics of iron ore. *Ironmaking Steelmaking* **2002**, *29*, 91−95.

(2) Ueda, S.; Kon, T.; Miki, T.; Kim, S. J.; Nogami, H. Effects of Al_2O_3 and MgO on softening, melting, and permeation properties of CaO-FeO-SiO_2 on a coke bed. *Metall. Mater. Trans. B* **2016**, *47*, 2371−2377.

https://doi.org/10.1021/acsomega.1c06722
ACS Omega 2022, 7, 8686−8696

(3) Shen, F. M.; Zheng, H. Y.; Jiang, X.; Wei, G.; Wen, Q. L. Influence of Al_2O_3 in blast furnace smelting and discussions on proper w(MgO)/w(Al_2O_3) ratio. *Iron Steel* **2014**, *49*, 1−6.
(4) Jiang, C.; Li, K.; Zhang, J.; Qin, Q.; Liu, Z.; Liang, W.; Sun, M.; Wang, Z. Molecular dynamics simulation on the effect of MgO/Al_2O_3 ratio on structure and properties of blast furnace slag under different basicity conditions. *Metall. Mater. Trans. B* **2019**, *50*, 367−375.
(5) Wen, Q.; Shen, F.; Yu, J.; Jiang, X.; Gao, Q. Activity of CaO in CaO-$SiOe_2$-Al_2O_3-MgO slags. *ISIJ Int.* **2018**, *58*, 792−798.
(6) Pimenta, H. P.; Seshadri, V. Characterisation of structure of iron ore sinter and its behaviour during reduction at low temperatures. *Ironmaking Steelmaking* **2002**, *29*, 169−174.
(7) Yi, Z.; Liu, Q.; Shao, H. Effect of MgO on Highly Basic Sinters with High Al_2O_3. *Mining Metallurgy Exploration* **2021**, *38*, 2175−2183.
(8) Zhang, F. Study on low sintering ratio production of No.2 BF in An Gang Group. *Metallurgical Economy Manage.* **2019**, *06*, 34−37.
(9) Gao, F.; Zhang, Y. Z. Production practice of low sinter ratio of Baowu Steel Group No. 3BF. *Ironmaking* **2017**, *36*, 43−46.
(10) Cui, X. D.; Hu, J. B.; Si, X. G. Countermeasures to the great change of BF raw material conditions. *Hebei Metallurgy* **2019**, *01*, 21−24.
(11) Sinha, M. S.; Nistala, H.; Chandra, S.; Mankhand, T. R.; Ghose, A. K. Correlating mechanical properties of sinter phases with their chemistry and its effect on sinter quality. *Ironmaking Steelmaking* **2016**, *44*, 100−108.
(12) Umadevi, T.; Nelson, K.; Mahapatra, P. C.; Prabhu, M.; Ranjan, M. Influence of magnesia on iron ore sinter properties and productivity. *Ironmaking Steelmaking* **2009**, *36*, 515−520.
(13) Takeuchi, N.; Iwami, Y.; Higuchi, T.; Nushiro, K.; Oyama, N.; Sato, M. Evaluation of sinter quality for improvement in gas permeability of blast furnace. *ISIJ Int.* **2014**, *54*, 791−800.
(14) Liu, Z.; Niu, L.; Zhang, S.; Dong, G.; Wang, Y.; Wang, G.; Kang, J.; Chen, L.; Zhang, J. Comprehensive technologies for iron ore sintering with a bed height of 1000 mm to improve sinter quality, enhance productivity and reduce fuel consumption. *ISIJ Int.* **2020**, *60*, 2400−2407.
(15) Harvey, T.; Honeyands, T.; O'dea, D.; Evans, G. Study of sinter strength and pore structure development using analogue tests. *ISIJ Int.* **2020**, *60*, 73−83.
(16) Umadevi, T.; Deodhar, A. V.; Mahapatra, P. C.; Prabhu, M.; Ranjan, M. Influence of coating granulation process on iron ore sinter quality and productivity. *Steel Res. Int.* **2010**, *81*, 716−723.
(17) Xing, X.; Du, Y.; Zheng, J.; Wang, S.; Ren, S.; Ju, J. Isothermal carbothermal reduction of $FeTiO_3$ doped with MgO. *JOM* **2021**, *73*, 1328−1336.
(18) Jiang, X.; Yu, J. X.; Wang, L.; Xiang, D. W.; Gao, Q. J.; Zheng, H. Y.; Shen, F. M. Distribution of reformed coke oven gas in shaft furnace. *J. Iron Steel Res. Int.* **2020**, *27*, 1382−1390.
(19) Webster, N.; Pownceby, M. I.; Manuel, J. R.; Pattel, R.; Kimpton, J. A. Fundamentals of silico-ferrite of calcium and aluminum (SFCA) and SFCA-I iron ore sinter bonding phase formation: effects of MgO on phase formation during heating. *JOM* **2021**, *73*, 299−305.
(20) Wang, G.; Kang, J.; Zhang, J.; Wang, Y. Z.; Wang, Z. Y.; Liu, Z. J.; Xu, C. Y. Softening-melting behavior of mixed burden based on low-magnesium sinter and fluxed pellets. *Int J Miner Metall Mater* **2021**, *28*, 621−628.
(21) Yang, N.; Guo, X. M.; Saito, N.; Nakashima, K.; Zhao, J. T. Effect of MgO on formation and crystallization behaviors of calcium ferrite during heating and cooling processes. *ISIJ Int.* **2018**, *58*, 1406−1412.
(22) Pan, F.; Zhu, Q.; Du, Z.; Sun, H. Migration behavior of the MgO and its influence on the reduction of Fe_3O_4-MgO sinter. *ISIJ Int.* **2018**, *58*, 652−659.
(23) Yu, B.; Lv, X.; Xiang, S.; Bai, C.; Yin, J. Wetting behavior of calcium ferrite melts on sintered MgO. *ISIJ Int.* **2015**, *55*, 1558−1564.
(24) Nandy, B.; Chandra, S.; Bhattacharjee, D.; Ghosh, D. Assessment of blast furnace behaviour through softening-melting test. *Ironmaking Steelmaking* **2006**, *33*, 111−119.
(25) Jiang, D. J.; Lin, Q. G.; He, M. G.; Gan, Q.; Fu, W. G. Effect of MgO on smelting performance and process parameters of sinter and blast furnace slag. *China Metall.* **2010**, *20*, 35.
(26) Shen, F.; Jiang, X.; Wu, G.; Wei, G.; Li, X.; Shen, Y. Proper MgO addition in blast furnace operation. *ISIJ Int.* **2006**, *46*, 65−69.
(27) Kasai, E.; Sakano, Y.; Kawaguchi, T.; Nakamura, T. Influence of properties of fluxing materials on the flow of melt formed in the sintering process. *ISIJ Int.* **2000**, *40*, 857−862.
(28) Hsieh, L. H. Effect of raw material composition on the sintering properties. *ISIJ Int.* **2005**, *45*, 551−559.
(29) Cores, A.; Babich, A.; Muñiz, M.; Ferreira, S.; Mochon, J. The influence of different iron ores mixtures composition on the quality of sinter. *ISIJ Int.* **2010**, *50*, 1089−1098.
(30) Jiang, X. Doctor Thesis. *Basic theoretical study on rational utilization of MgO containing raw materials in blast furnace burden*; Northeastern University, China: 2008.
(31) Han, H. S.; Shen, F. M.; Jiang, X.; Bi, C. G.; Zheng, H. Y.; Gao, Q. J. Fundamental mechanism of effects of MgO on sinter strength. *J. Iron Steel Res. Int.* **2019**, *26*, 1171−1177.
(32) Zhu, D.; Chou, J.; Shi, B.; Pan, J. Influence of MgO on low temperature reduction and mineralogical changes of sinter in simulated COREX shaft furnace reducing conditions. *Minerals* **2019**, *9*, 272−282.
(33) Zhou, M.; Yang, S. T.; Jiang, T.; Xue, X. X. Influence of MgO in form of magnesite on properties and mineralogy of high chromium, vanadium, titanium magnetite sinters. *Ironmaking Steelmaking* **2015**, *42*, 217−225.
(34) Zhang, J. L.; Liu, D. H.; Wang, X.; Liu, L.; Jiang, Z. J. X. Present situation and development direction of sinter chemical composition control. *Sintering Pelletizing* **2017**, *42*, 1−5.

https://doi.org/10.1021/acsomega.1c06722
ACS Omega 2022, 7, 8686−8696